Pesquisas em Geociências, v. 49 (2022), n. 2: 118014 E-ISSN 1807-9806
Instituto de Geociências, Universidade Federal do Rio Grande do Sul, Porto Alegre, RS, Brasil doi.org/10.22456/1807-9806.118014

Effects of Tropospheric Refraction on Precise Point Positioning in Brazil

Franciele Lúcia Silva BRAGA[1], William Rodrigo Dal POZ[1,2]

[1] Postgraduate Program in Civil Engineering, Federal University of Viçosa, Peter Henry Holfs Avenue, s/n, University Campus, Zip code 36570-900, Viçosa-MG, Brazil (franciele.braga@ufv.br)
[2] Federal University of Viçosa, Center for Exact Sciences, Department of Civil Engineering, Graduate Program in Civil Engineering, Campus Viçosa, Peter Henry Holfs Avenue, s/n, University Campus, Zip code 36570-900, Viçosa-MG, Brazil (william.dalpoz@ufv.br)

Abstract. Troposphere is one of the most limiting sources of error in the accuracy of Precise Point Positioning method. This work aims to analyze the effects of tropospheric delay on this positioning belonging to the Brazilian Network for Continuous Monitoring of Global Navigation Satellite Systems (GNSS). The tropospheric delay is generated by the influence of the hydrostatic and dry atmosphere. Corresponds to about 2.3 m at zenith for hydrostatic component, 1 to 35 cm at zenith for wet component. Although the wet component is generally smaller, its temporal and spatial variation is much greater, which makes its modeling difficult. GNSS data are related to several climatic zones, including Amazon region, referring to four seasons. The data were processed considering six strategies, each one using different troposphere models and mapping functions for analysis. Results were evaluated according to the Root Mean Square, estimated for 15 processing days for each season, involving 89 GNSS stations. For the planimetric result, the best result was obtained in the frequency histogram in which the Hopfield model was used for the hydrostatic component and the Hopfield mapping function for the estimated wet component (5% of the sample with an accuracy greater than 3 cm). The best processing method in relation to the altimetric component was obtained using the Vienna mapping function - VMF1, together with the Zenith Tropospheric Delay (ZTD) corrections based on the Numerical Weather Forecast/European Center for Medium-Range Weather Forecast (NWF /ECMWF) model (94.2% of the sample accuracy less than 3 cm). Results show that the greatest effects of the tropospheric delay occurred in the equatorial region, related to the altimetric component, in all seasons of the year. This climatic zone is under a strong influence of the Amazon region, which presents high annual humidity values. In addition, it can occur a great humidity variation in this region, which can compromise the process of estimating wet component of tropospheric delay. Finally, results showed that the best processing strategy was the use of the Vienna mapping function in conjunction with corrections based on the Numerical Weather Forecast model.

Keywords: Bernese GNSS Software, Mapping Functions, PPP, Tropospheric Models, and Zenith Tropospheric Delay.

Resumo. EFEITOS DA REFRAÇÃO TROPOSFÉRICA NO POSICIONAMENTO POR PONTO PRECISO NO BRASIL. A troposfera é uma das fontes de erro mais limitantes na acurácia do método de Posicionamento por Ponto Preciso. Este trabalho tem como objetivo analisar os efeitos do atraso troposférico nesta técnica de posicionamento a dados do *Global Navigation Satellite Systems* (GNSS) pertencentes à Rede Brasileira de Monitoramento Contínuo de Sistemas GNSS. O atraso troposférico é gerado pela influência da atmosfera hidrostática e seca. Corresponde a cerca de 2,3 m no zênite para componente hidrostática, 1 a 35 cm no zênite para componente úmida. Apesar, da componente úmida ser geralmente menor, sua variação temporal e espacial é muito maior, o que dificulta a sua modelagem. As observáveis GNSS estão relacionadas a várias zonas climáticas, incluindo a região amazônica, referindo-se às quatro estações do ano. Os dados foram processados considerando seis estratégias, cada uma usando diferentes modelos troposféricos e funções de mapeamento para análise. Os resultados foram avaliados segundo EMQ (Erro Médio Quadrado), estimado para 15 dias de processamento para cada estação, envolvendo 89 estações GNSS. Para a resultante planimétrica, o melhor resultado foi obtido no histograma de frequências em que foi utilizado o modelo Hopfield para componente hidrostática e a função de mapeamento Hopfield para a componente úmida estimada (5% da amostra com acurácia maior que 3 cm).O melhor método de processamento em relação a componente altimétrica, foi obtida empregando a função de mapeamento de Vienna - VMF1, juntamente com as correções do atraso troposférico total (ZTD) baseadas no modelo de Previsão Numérica de Tempo do European Center for Medium-Range Weather Forecast -PNT/ECMWF- (94,2% da amostra de acurácia menor que 3cm). Os resultados mostram que os maiores efeitos do atraso troposférico ocorreram na região equatorial, relacionados à componente altimétrica, em todas as estações do ano. Esta zona climática é fortemente influenciada pela região amazônica, que apresenta altos valores anuais de umidade. Além disso, nesta região pode haver uma grande variação de umidade, o que pode comprometer o processo de estimativa da componente úmida do atraso troposférico. Por fim, os resultados mostraram que a melhor estratégia de processamento foi utilizar a função de mapeamento de Viena em conjunto com as correções baseadas no modelo de Previsão Numérica do Tempo.

Palavras-chave: Software Bernese GNSS, Funções de Mapeamento, PPP, Modelos Troposféricos, Atraso Troposférico Zenital.

1 Introduction

Due to the use of data from dual-frequency receivers in processing of Global Navigation Satellite Systems (GNSS) data, the effects of ionosphere are no longer the largest source of error in positioning by this system, even to determine Precise Point Positioning (PPP), because of the application of ionosphere-free combination. As a result, troposphere has become one of the most important and limiting source of errors in PPP accuracy (Xiong *et al.*, 2019). The disturbance caused by troposphere in GNSS (in units of length) is the tropospheric delay (also known as tropospheric refraction). When satellite is at zenith and GNSS station is at sea level, in standard atmospheric conditions, tropospheric delay can be close to 2.3 meters (Dach *et al.*, 2015). For a satellite near the horizon, signal delay caused by troposphere, in distance domain, can reach 30 meters (Sanz Subirana *et al.*, 2013) or more (Xu and Xu, 2016).

Tropospheric delay is modeled as a product of zenith tropospheric delay (ZTD) and as a geometric factor, called mapping function, which describes dependence of delay as a function of elevation angle (Niell, 1996). Thus, mapping functions at a given zenith angle (or elevation angle) project zenith tropospheric delay along satellite direction (Collins & Langley, 1999). Several models of mapping functions can be used to relate inclined tropospheric delay, such as the simple mapping function 1 / cos (Z) (Saastamoinen, 1972), suitable for zenith angles (Z) up to 70 ° (Saha *et al.*, 2010). Others, such as the functions developed by Marini (1972); Ifadis (1986); Herring (1992); Niell (1996); Foelsche & Kirchengast (2002); Böhm *et al.* (2006a), Böhm *et al.* (2006b) and Landskron & Böhm (2017) can be used for greater zenith angles.

ZTD depends, basically, on temperature, pressure and relative air humidity (Sanz Subirana *et al.*, 2013). It has two main components: hydrostatic and wet. Zenith hydrostatic delay (ZHD) corresponds to 90% of tropospheric delay (Zhao *et al.*, 2018) and it is modeled based on both temperature and pressure of the observation site, which can be obtained from a standard atmosphere model or from meteorological surface data (Karabatic, 2009). Although zenith wet delay (ZWD) generates less influence than the hydrostatic one, it is extremely difficult to model or determine distribution of water vapor in the atmosphere, since water vapor density varies widely with position and time (Spilker, 1996). Given this difficulty, the ability to correct the ZWD becomes a critical factor, given its non-linear or non-homogeneous distribution and its susceptibility to changes, due to high temporal variability, which can reach 20% in a few hours (Teunissen & Kleusberg, 1998; Spilker, 1996).

Thus, in the process of modeling tropospheric delay of PPP, ZHD may be precisely predicted from an a priori troposphere model. In contrast, ZWD is estimated during GNSS processing along with other unknown parameters, such as position coordinates (Dach *et al.*, 2015). Tropospheric horizontal gradients with two components can also be considered, in North-South and East-West directions (Bar-Sever *et al.*, 1998; IERS, 2010). In this case, total tropospheric delay in sight line (satellite-receiver) is obtained from the sum of hydrostatic and wet delays in zenith direction, multiplied by respective mapping functions, with a gradient correction. These corrections are important for observations collected by satellites with a low elevation angle (Chen & Herring, 1997).

This methodology can be applied, for example, in the scientific data processing program GNSS Bernese (BSW), used in this work. Bernese is known for providing high quality results for geodetic applications. It was developed by the Astronomical Institute at the University of Bern, Switzerland, offering a wide variety of tropospheric delay models and mapping functions. The Bernese GNSS Software consists of more than 450,000 lines of Fortran source code in about 1,500 modules. Bernese's software allows for the creation of an automated processing file, called the Processing Control File (PCF), which lists all programs to be executed in a certain sequence or in parallel. The PCF file runs through the Bernese Processing Engine (BPE), a service for automated, interactive and non-interactive processing. Data processing consists of several steps, including data import, orbit preparation, clock synchronization, cycle slip detection, and parameter estimation. Consistency of the introduced orbit, Earth orientation parameters (EOPs) and satellite clock information is of utmost importance to achieve high accuracy. It is mandatory to use the information from the same source. Mixing orbits and clocks from different Analysis Centers degrades PPP results (Dach *et al.*, 2015).

In Brazil, some research carried out on the impacts of tropospheric models on GNSS positioning can be highlighted, such as those by Gouveia *et al.* (2014 and 2017), Cherubim *et al.* (2016), Abreu *et al.* (2014), Oliveira *et al.* (2014) and Alves *et al.* (2016). Among the most recent studies carried out in other countries, involving evaluation of tropospheric models in PPP, we can highlight the work carried out by Wang & Li (2016), Pan & Guo (2018), Xiong *et al.* (2019) and Tunali & Ozludemir (2019).

The contribution of these articles will be described below. In Gouveia *et al.* (2017) an evaluation was carried out considering two years of data (2012 and 2013) and 5 RBMC stations, located in different regions of Brazil, with the objective of evaluating the convergence time of the PPP initialization and the positioning accuracy when using the Hopfield and Zenital Tropospheric Delay (ZTD) models/ Center for Weather Prediction and Climate Studies of the National Institute for Space Research (CPTEC). The results indicate that the greatest gain when using Numerical Weather Forecast (NWF) refers to the accuracy of the coordinates, since there was a significant improvement in the quality of the results.

In Gouveia *et al.* (2014) the impact of improvements in the quality of the neutrospheric zenith (ZND) predictions was determined, in order to present a robust evaluation of the available versions, using as a reference the ZND values estimated from the GNSS data collected by the RBMC stations, taking into consideration: seasonal variation, continentality and variation in altitude and latitude.

Cherubim *et al.* (2016) provides details of the processing and adjustment of an experiment with GNSS data from stations Coari, Cruzeiro do Sul, São Luís, Natal, Cuiabá, Brasília, Vitória, Chapecó, Curitiba and Porto Alegre, belonging to RBMC selected at different times, stations of the year and geographic locations, in order to investigate the impact of global empirical models of the Troposphere such as Hopfield and Saastamoinen on high precision geodetic positioning. The results showed that there are no statistically significant differences in the performance of these two models.

In Abreu *et al.* (2014) was evaluated and quantified the wet component of the tropospheric delay in different regions of Brazil using RBMC data. It was observed that the highest values of ZWD were obtained at the SAGA station and the lowest at the UFPR station. An evaluation was also carried out regarding the use of the eta15km NWF model in point positioning. The results showed that using the NWF model instead of Hopfield brings significant improvements in positioning.

In Oliveira *et al.* (2014) comparative tests were carried out in the four seasons of the year with the regional tropospheric model of NWF /INPE/ECMWF. In addition, the VMF1 mapping function has been implemented and tested for the different models. In the quality analysis of the Virtual Reference Station (VRS) data, the PPP method provided satisfactory results in both static and kinematic modes. The P NWF/INPE model showed an average improvement of 29.7 and 31.7% in relation to the NWF/ECMWF for dry and wet days, respectively.

Alves *et al.* (2016) evaluated the numerical weather forecast (NWP) model for South America, known as Eta from CPTEC/INPE (Center for Weather Forecasting and Climatic Studies/Brazilian Institute for Space Research). This NWP model was evaluated in precise point positioning (PPP) and network-based positioning. For network-based positioning, the best results were obtained mainly when the tropospheric characteristics are critical, in which case an improvement of up to 7.2 % was obtained in 3D RMS using NWP models. Concerning PPP, the best positioning results were obtained for the station SAGA, located in region. Using the NWP model, the 3D RMS are less than 10 cm for all 24 hours of data, whereas the values reach approximately 60 cm for the Hopfield model.

Wang & Li (2016) evaluate the accuracy of three tropospheric delay models, together with five mapping functions in wet delays calculation. The evaluations are conducted by comparing their slant wet delays with those measured by water vapor radiometer based on its satellite-tracking function (collected data with large liquid water path is removed). For all 15 combinations of three tropospheric models and five mapping functions, their accuracies as a function of elevation are statistically analyzed by using nine-day data in two scenarios, with and without meteorological data.

Pan & Guo (2018) evaluated ZTDs retrieved from different constellation combinations (i.e. GPS/GLONASS/Galileo/BDS, GPS/GLONASS and GPS only), different processing models for ionospheric delays (i.e. no ionosphere (IF)) combined PPP and uncombined PPP (UC) and different modes (i.e. real-time mode and post-processing mode) are compared.

Xiong *et al.* (2019) was evaluated along with the ZTD and horizontal gradients, the carrier phase residuals from PPP backward filter are considered to reconstruct slant tropospheric delay (STD). Based on the proposed STD model, its marginal effects on GPS PPP were investigated. Results indicated that the consideration of carrier phase residuals for STD modeling can improve the three-dimensional accuracy to 0.5, 1, 1.2 cm in the South, North,Up (N, E, U) components.

Tunali & Özlüdemir (2019) processed a set IGS stations within the area affected by the central European Flooding 2013 and assessed the performance of post-processed PPP during severe weather by applying different troposphere models: VMF1 together with the ECMWF grids, the GMF with the Global Pressure and Temperature 2, the NMF with the University of New Brunswick (UNB), and the VMF1 with the UNB/VMF1 from the National Centers for Environmental Prediction numerical weather model (NWM) data. Wet delay estimates from each PPP session have been verified through the IGS final troposphere products, local surface measurements and double-differenced (DD) GNSS solutions performed at the same sites. All the PPP solutions agree well with the IGS.

None of these studies presented an integrated analysis of the effects of troposphere on PPP, considering the following aspects: analysis of effects of tropospheric delay on PPP using Bernese, based on GNSS data belonging to the Brazilian Network for Continuous Monitoring of GNSS Systems (RBMC), which come from GNSS stations distributed throughout Brazilian territory (a large country) and include several climatic zones (including Amazon region) in four seasons of the year.

The general objective of this research is to analyze the effect of tropospheric refraction on the PPP in Brazilian territory, and to indicate the best strategy for the reduction of tropospheric delays. Under these conditions, with technological innovation, updating of more robust positioning software, in addition to the availability of data from active GNSS networks to the public by government agencies and/or research centers, there is an interest in analyzing the effect of tropospheric delay in processing. of GNSS observations for the five geographic regions of Brazil, using different models for tropospheric refraction available in the BERNESE GNSS v.5.2 software.

2 Materials and methods

As Brazil is a country with continental characteristics, with different climates and different indices of air humidity and temperature, throughout its extension and year, we tried to carry out experiments in each of the climatic zones or regions of Brazil, being: Equatorial, Temperate, Tropical Central Brazil, Tropical Equatorial and Tropical Eastern Northeast (Nimer, 1979). Thus, 89 GNSS stations from RBMC were selected, whose spatial distribution are shown in Figure1. It is important to highlight that there is no single way to define climatic zones, since several criteria can be adopted for this purpose. However, as all the GNSS receivers used in this work are installed in the Brazilian region, it was decided to use the regional definition given by Nimer (1979).

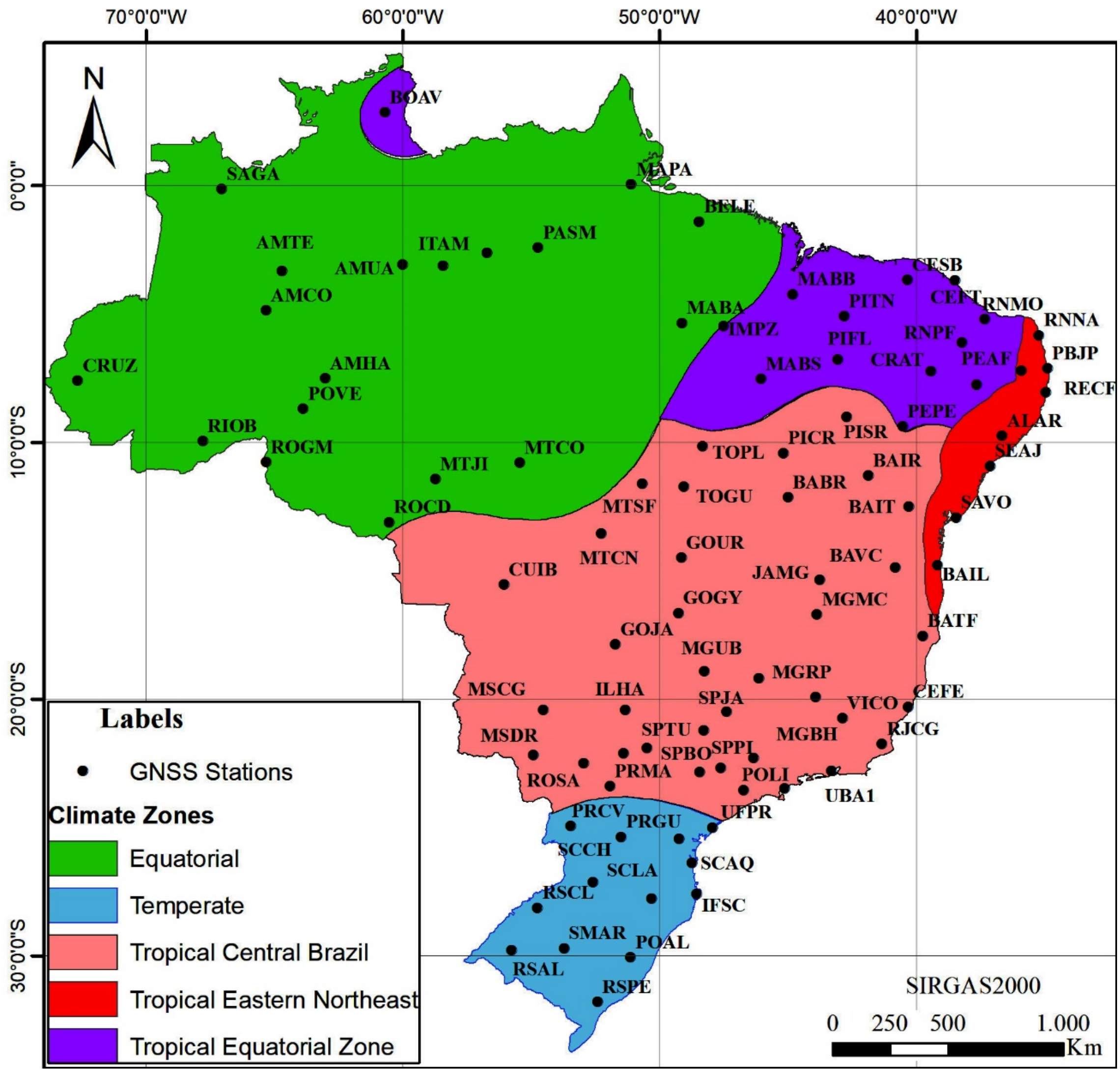

Figure 1. Spatial distribution of RBMC stations used in this study. Source. (Adapted by the authors based on Nimer (1979)). Available at https://educa.ibge.gov.br/images/educa/clima.pdf).

Figura 1. Distribuição espacial das estações da RBMC usadas neste estudo. Fonte. (Adaptado pelos autores com base em Nimer (1979)). Disponível em: https://educa.ibge.gov.br/images/educa/clima.pdf).

This study used the International GNSS Service (IGS) Final Products, including the IGS final orbit, Clocks and Earth Orientation Parameters (ERP). Differential Code Biases (DCBs) files and the Global Ionosphere Maps of the Center for Orbit Determination in Europe (CODE) were also used. Ocean tide loading model parameters were obtained from the web-service available at: Bos and Scherneck (2013). Atmospheric tidal loading file was generated using Bernese, based on the model by Ray & Ponte (2003). Coefficients of Vienna Mapping Function 1 (VMF1, 2017) were used as well. These parameters are provided in a global grid (2.0° latitude x 2.5° longitude) every six hours, which is the usual temporal resolution of data from the European Center for Medium-Range Weather Forecast (ECMWF). The coefficients of the other mapping functions used in this work are already implemented in the Bernese software. As mentioned, processing of observables GNSS was carried out in Bernese, version 5.2.

Matlab software version R2012b performed the routine for transforming reference frames and updating coordinates, in addition to calculations of discrepancies, precision, and planimetric and altimetric accuracy.

In carrying out this work, GNSS observables (RINEX files) were used with 24-hours tracking interval, for 60 days of the year 2016, distributed equally for each season. Therefore, data collected during 15 continuous days of GNSS observations in summer, autumn, winter and spring were processed (Table 1). The Table 2 presents a summary of some parameters used in the processing performed in Bernese.

Table 1. Processing periods by season.
Tabela 1. Períodos selecionados para o processamento em cada estação do ano.

Seasons	Processing range	*DOY	Central Epoch (years)
Summer	2016/01/28 to 2016/02/11	28 to 42	2016.096
Autumn	2016/04/28 to 2016/05/12	119 to 133	2016.344
Winter	2016/07/30 to 2016/08/13	212 to 226	2016.598
Spring	2016/10/30 to 2016/11/13	304 to 318	2016.956

** **DOY**: Day of Year.*
** **DOY**: Dia do ano.*

Table 2. BSW processing strategy – v.5.2.
Tabela 2. Estratégia de processamento no BSW – v.5.2.

Parameter	Description
Observation Interval	30 seconds
Orbital Products	IGS and IGL final / precise
Ocean Tidal Loading	FES2004
Atmospheric Tidal Loading	Ray & Ponte (2003)
Solid Earth Tides	IERS, 2010
Phase Center Offsets and variations of satellite antennas	PCV.I08 (ANTEX *format*)
Phase Center Offsets and variations of receiver antennas	PCV.I08 (ANTEX *format*)
Elevation Mask	3°
Reference Frame	ITRF2008
GNSS Systems	GPS and GLONASS
Ionosphere	Ionosphere–Free Linear Combination (L3)
Mapping function	GMF, NIELL, VMF1, Hopfield, $\frac{1}{\cos Z}$
Wet component of Tropospheric Delay	Estimated
Horizontal Gradients	Estimated
Gradient Model	CHENHER (Chen & Herring, 1997)
Processing method	PPP

2.1 A priori models and corresponding mapping functions

This software offers several a priori models and corresponding mapping functions to correct tropospheric delay. In version 5.2, the following models and mapping functions are available:

- Global Mapping Function (GMF), hydrostatic and wet, in which ZTD corrections are calculated based on the Global Pressure and Temperature model (GPT) and the Saastamoinen model;
- The Vienna Mapping Function 1 (VMF1), hydrostatic and wet, together with ECMWF-based ZTD corrections;
- The Niell model (1996), hydrostatic and wet, in which ZTD corrections are calculated based on the Saastamoinen model together with the Niell Mapping Functions (NMF), which is recommended for analyzing GNSS data with low elevation angle;
- The Saastamoinen model; and
- The modified Hopfield model.

One of the most popular models for calculating tropospheric refraction is the empirical model of Saastamoinen (1972) based on the laws associated with an ideal gas. The model adopts the premise of hydrostatic equilibrium conditions (Saastamoinen, 1972; Monico, 2008).

In the tropospheric delay model developed by Hopfield (1969), the hydrostatic and wet refractivity components are a function of the values of temperature, pressure, and the height of the atmospheric layer (H) that interferes in the propagation of electromagnetic signals, in relation to the station of tracking (Sapucci & Monico, 2001; Seeber, 2003).

The PNT/ECMWF requires the continuous input of surface meteorological data, obtained from satellites, ground observations, automatic stations, aircraft, buoys, ships, remote sensing data and radiosonde, in order to provide current forecasts, and climate reanalysis. The model has a resolution of 0.25°x0.25° with 21 vertical levels. In this way, the tropospheric delay for a given position is obtained by performing a bilinear interpolation for the position of the station using the grid values (Oliveira *et al.*, 2014). The ZTD values from the ECMWF model are available together with the coefficients from the Vienna mapping function.

The empirical GPT model developed by Böhm *et al.* (2007), provides pressure and temperature values in the vicinity of the earth's surface, which are used to calculate a priori estimates of the hydrostatic component of the tropospheric delay. This model is an adjustment in spherical harmonics up to degree and order 9 and has as input parameters the geodetic coordinates of the station and the day of the year.

The Niell Mapping Function (NMF), introduced in 1996 by Niell (1996), is based on changes in time and geographic location rather than surface meteorological parameters.

Vienna mapping functions (VMF) was developed in ECMWF by Böhm & Schuh (2004) and is based on the PNT/ECMWF model. The VMF coefficients make it possible to determine the tropospheric delay for an initial elevation $\mathcal{E}$ of 3.3 degrees. The VMF was updated by Böhm *et al.* (2006b) and was named VMF1. In this update, the coefficients bh and ch are derived by least squares fit from one-year ECMWF data, where bh is a constant and ch depends on DOY and latitude.

The GMF was developed by Böhm *et al.* (2006a), and similar to GPT uses 15°×15° grids of average monthly pressure, temperature and humidity profiles from ECMWF reanalysis data (ERA40). The coefficients b and c are obtained from empirical equations of the VMF1 function, while the hydrostatic and wet coefficients are obtained from an expansion in spherical harmonics.

It is worth mentioning, however, that for a first order all functions and mapping can be approximated by Equation 1 (Dath *et al.*, 2015):

$$F(z) = \frac{1}{\cos(Z)} \qquad (1)$$

Where Z is the zenith angle.

In order to analyze the impact of tropospheric models on PPP, several strategies for final solution were investigated, according to the models and mapping functions available in BSW. Table 3 shows the processing strategies performed at BSW regarding the mitigation of tropospheric delay. For each processing strategy, a priori model associated with a mapping function for the hydrostatic component of the tropospheric delay was chosen. In addition, a mapping function for the wet component was also chosen, to be predicted with the other parameters in the least-square adjustment. There is a great correlation when estimating together the troposphere parameters, station height and receiver clock. This correlation decreases as the elevation angle is reduced, assuming a uniform distribution of the GNSS satellites (Dach *et al.*, 2015). For this reason, the value of 3° was adopted for the elevation mask in all processing strategies, in order to consider observations from satellites close to the horizon. However, when using measurements with low elevation angles, it is recommended to estimate horizontal tropospheric gradients, which was also considered in the strategies.

Table 3. Processing strategies for mitigating tropospheric delay.
Tabela 3. Estratégias de processamento para mitigação do atraso troposférico.

Strategy	A priori tropospheric model (model + *MF**)	*MF* to ZWD*
1	No tropospheric corrections for ZHD	$\frac{1}{\cos Z}$
2	Saastamoinen	NMF_{wet}
3	Hopfield	Hopfield
4	Niell (Saastamoinen $_{Dry}$ with NMF_{Dry})	NMF_{wet}
5	GPT_{Dry} with GMF_{Dry}	GMF_{wet}
6	$ECMWF_{Dry}$ with $VMF1_{Dry}$	$VMF1_{wet}$

Strategy 1, in which a priori model was not used to correct the hydrostatic component, is partially without tropospheric correction (around 90%), since the wet component was estimated. For this processing strategy, the simplest mapping function (1/cosZ) was chosen for the wet component.

To analyze which processing strategy in Table 3 performed best, an analysis of the accuracy of estimated coordinates for each tropospheric delay model was performed. The calculation of daily planimetric and altimetric accuracy can be obtained in accordance with equations 2 and 3, respectively:

$$\mathrm{RMSE}_{p} = \sqrt{{D_p}^2 + {\sigma_p}^2} \quad (2)$$

$$\mathrm{RMSE}_{h} = \sqrt{{D_h}^2 + {\sigma_h}^2} \quad (3)$$

Where; D_p: Planimetric discrepancy of geodetic coordinates, in meters; σ_p: Precision of the resulting planimetric geodetic coordinates, in meters; D_h: Altimetric discrepancy, in meters; and σ_h: Altimetric precision, in meters. The precision values used correspond to only the estimated solution (daily) and assume the precision of the reference solution to be negligible.

$$\sigma_p = \sqrt{{\sigma_N}^2 + {\sigma_E}^2} \quad (4)$$

In this equation, σ_N, σ_E represent the precision in north and east, respectively. These are precisions in north and east coordinates in meters, obtained from the propagation of global Cartesian coordinates.

Planimetric and altimetric discrepancies result from the simple difference between BSW estimated coordinates and reference coordinates, which are made available by Brazilian Institute of Geography and Statistics

(IBGE) in their respective descriptions, SIRGAS2000 reference epoch 2000.4 years (Waldhelm *et al.*, 2006). However, coordinates of reference stations need to be in the same reference frame as estimated coordinates, just as it is necessary to be compatible in terms of epoch, in order to reduce the effect of displacement among tectonic plates. The satellites coordinates obtained using the precise ephemeris of IGS were referenced to IGb08 (ITRF2008) until GPS week 1933, so that coordinates estimated in this study are referenced to IGb08 as well. For this reason, reference coordinates in SIRGAS2000, epoch 2000.4, of RBMC stations were transformed and updated to ITRF2008, at epoch of GNSS data. Transformation parameters provided by the Institut National de L'Information Géographique et Forestière (IGN) (IGN, 2017) were used, as they allow to change the reference and update the coordinates according to the various ITRFs. In this work, the alignment between IGb08 and ITRF2008 (Bruyninx *et al.*, 2013), and between SIRGAS2000 and ITRF2000 (Weston & Soler, 2012) are considered. Equations 5 to 7 demonstrate how discrepancies of planimetric accuracy were obtained, in metric units, considering the GRS80 ellipsoid. The transformation of angular discrepancies in degrees (Dφ and Dλ) to linear discrepancies in meters (D_N and D_E) can be obtained as in Torge & Muller (2012).

$$\begin{vmatrix} \mathrm{D_N} \\ \mathrm{D_E} \end{vmatrix} = \begin{vmatrix} N_{(est)} - N_{(ref)} \\ E_{(est)} - E_{(ref)} \end{vmatrix} \quad (5)$$

$$D_p = \sqrt{\mathrm{D_N}^2 + \mathrm{D_E}^2} \quad (6)$$

And altimetric discrepancy in meters is given by Equation 7:

$$D_h = h_{est} - h_{ref} \quad (7)$$

A clustered altimetric accuracy of 15 days or clustered RMSE is also calculated for each season referring to the 15 days of processing in the summer, autumn, winter and spring periods. It is noteworthy that the reference position adopted stems from the old SIRGAS campaign carried out from May 10 to 19, 2000 (Costa *et al.*, 2002). The use of the SIRGAS weekly solution is recommended, which would imply that h_ref in Equation (6) varies with the day of the year instead of being a constant.

Some characteristics adopted in the processing of the SIRGAS2000 campaign by the IBGE are described below (Costa *et al.*, 2002): An a priori tropospheric model was not used; tropospheric delay correction was estimated every 2 hours; use of Niell mapping function for hydrostatic component; estimation of tropospheric gradient parameters using the tilting mapping function; and resolution of ambiguities using the QIF (Quasi Ionosphere Free) strategy and the CODE global ionosphere maps, called GIMs (Global Ionosphere Maps), and the use of IGS orbital products. Thus, the configuration of the SIRGAS campaign processing is different from the PPP processing in the BSW of this study. Mainly by the positioning method, orbital products used, tropospheric delay a priori modeling, mapping function, gradient model, and the elimination of ionosphere effects.

The IERS (International Earth Rotation and Reference Systems Service) recommends that the hydrostatic delay be accurately calculated a priori based on reliable surface pressure data using the Saastamoinen (1972) formula given by Davis *et al.* (1985). Currently, there is no simple method for estimating a precise a priori value for the wet tropospheric delay, thus it is estimated with other parameters in the adjustment of observations. As for the tropospheric gradients, they can be obtained by the formula of Chen and Herring (1997). Regarding mapping functions, the VMF1 is recommended for any global application, such as determining ground reference and Earth orientation parameters (IERS, 2010).

3 Results and Discussion

Planimetric and altimetric accuracy was calculated for 89 GNSS stations of the Brazilian national network (RBMC), during 15 days for each season of 2016, as mentioned above. In order to present data in a more concise way, planimetric accuracy histograms will be presented, followed by those of altimetric accuracy, both in meters, according to each tropospheric delay model and mapping function identified in Table 3. Intervals and number of classes of histograms have been standardized to facilitate comparison of accuracy samples. Figures 2 and 3 show frequency histograms of resulting planimetric for each accuracy sample.

In Figure 2A, histogram of planimetric accuracy refers to strategy 1, in which a priori model for correction of hydrostatic component was not used, while wet component parameters of tropospheric delay were estimated in the least-square adjustment. In strategy 1, mapping function 1/cos(Z) was used for calculating wet component. This model was presented to the manuscript in order to show the magnitude of approximately 90% of the error due to tropospheric refraction when a model to correct the hydrostatic component of the tropospheric delay is not used. It can be seen in Figure 2A that 94.6% of results are below 3 cm. However, 0.5% of values were greater than 5 cm (5 to 18 cm). Figure2B shows frequency histogram of planimetric accuracy for strategy 2. In this strategy, a priori Saastamoinen model was used to correct hydrostatic component, and NMF_{Wet} mapping function was applied to estimated wet component. It should be noted that mapping functions are implicit in Saastamoinen model. Analyzing the histogram in Figure 2B, we can note that 93.2% of the sample of 5340 values are less than 3 cm, 23.8% being less than 1 cm (millimeter accuracy). On the other hand, 0.9% of sample presented values greater than 5 cm (5 to 12 cm). Figure 2C shows frequency histogram of resulting planimetric accuracy for strategy 3. In this strategy, a priori Hopfield model was used to correct hydrostatic component, and Hopfield mapping function was applied to estimated wet component. It appears that 95% of the 5,340 values sample showed results below 3 cm, while 32.1% of them obtained planimetric accuracy less than 1 cm. Only 0.3% of sample showed values greater than 5 cm (5 to 11 cm).

Figure 3A presents frequency histogram of resulting planimetric accuracy of coordinates for strategy 4. In this processing, the priori Niell model ($Saastamoinen_{Dry}$ associated with NMF_{Dry} mapping function) was used. For the wet component, NMF_{Wet} mapping function was used. By analyzing Figure 3A, we can note that 94.4% of sample had values lower than 3 cm. In addition, 0.4% of results of planimetric accuracy showed values greater than 5 cm (5 to 12 cm). Frequency histogram in Figure3B refers to planimetric accuracy of coordinates using a priori GPT hydrostatic model in conjunction with GMF_{Dry} mapping function. The GMF_{Wet} mapping function was chosen for analyzing wet component of tropospheric delay. For this strategy, 93.7% of sample presented planimetric accuracy values less than 3 cm, while 0.4% of sample showed values greater than 5 cm (5 to 9 cm). The frequency histogram in Figure3C represents the planimetric accuracy sample for strategy 6. The a priori model used for calculation of the hydrostatic component was the $ECMWF_{Dry}$ model together with the VMF1Dry mapping function. For the wet component, the $VMF1_{Wet}$ mapping function was used. It is noted that 94.2% of the planimetric accuracy sample for strategy 6 presented values below 3 cm. However, 0.4% of the accuracy was greater than 5 cm (5 to 9 cm).

When evaluating the 6 frequency histograms, we can conclude that in relation to planimetry the processing showed similar performance, even for a strategy in which a priori model for hydrostatic component was not used. However, the histogram of the strategy in which Hopfield model was used for hydrostatic component (Figure 2C) have obtained the highest percentage of planimetric accuracy below 3 cm, as well as the lowest percentage of values greater than 5 cm. On the other hand, processing using a priori Saastamoinen model (strategy 2) showed the lowest percentage of planimetric accuracy less than 3 cm, combined with the highest percentage of values greater than 5 cm.

a) Partially without correction

	Planimetric Accuracy (centimeters)	Frequency	
		Units	(%)
1	≤ 0.5	398	7.5
2	> 0.5 and ≤ 1.0	1384	25.9
3	> 1.0 and ≤ 3.0	3267	61.2
4	> 3.0 and ≤ 5.0	262	4.9
5	> 5.0	29	0.5
	Total:	5340	100

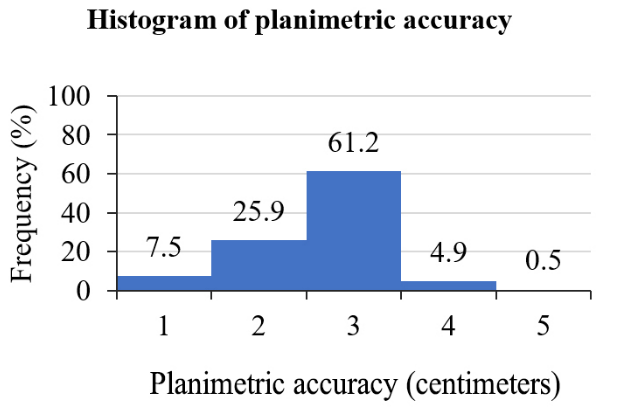

b) Saastamoinen

	Planimetric Accuracy (centimeters)	Frequency	
		Units	(%)
1	≤ 0.5	221	4.1
2	> 0.5 and ≤ 1.0	1054	19.7
3	> 1.0 and ≤ 3.0	3706	69.4
4	> 3.0 and ≤ 5.0	313	5.9
5	> 5.0	46	0.9
	Total:	5340	100

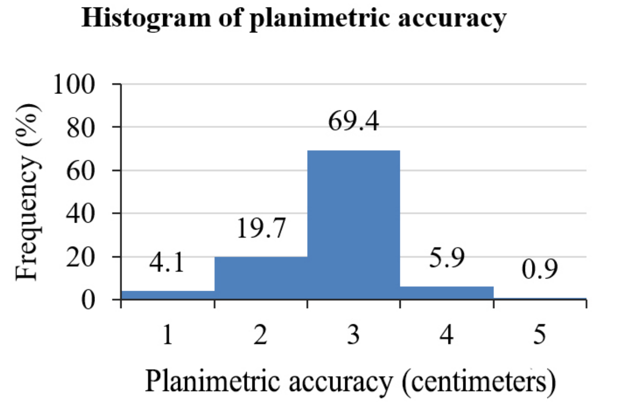

c)Hopfield

	Planimetric Accuracy (centimeters)	Frequency	
		Units	(%)
1	≤ 0.5	335	6.3
2	> 0.5 and ≤ 1.0	1379	25.8
3	> 1.0 and ≤ 3.0	3359	62.9
4	> 3.0 and ≤ 5.0	253	4.7
5	> 5.0	14	0.3
	Total:	5340	100

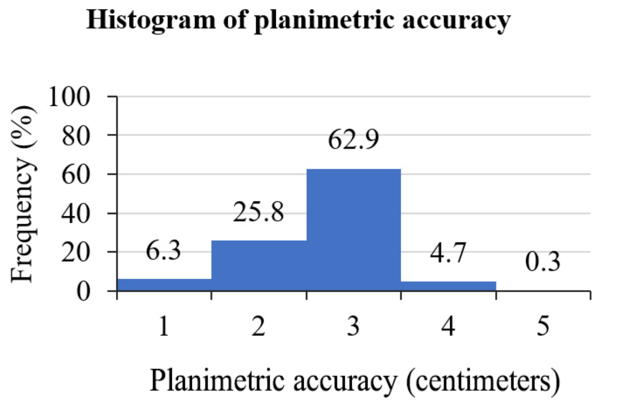

Figure 2. Histograms of planimetric accuracy samples (A) for strategy 1: Partially without correction; (B) for strategy 2: Saastamoinen; (C) for strategy 3: Hopfield.

Figura 2. Histogramas das amostras de acurácia planimétrica (A) para estratégia 1: Parcialmente sem correção; (B) para estratégia 2: Saastamoinen; (C) para estratégia 3: Hopfield.

a) $Saastamoinen_{Dry}$ with NMF_{Dry}

	Planimetric Accuracy (centimeters)	Frequency	
		Units	(%)
1	≤ 0.5	220	4.1
2	> 0.5 and ≤ 1.0	1273	23.8
3	> 1.0 and ≤ 3.0	3549	66.5
4	> 3.0 and ≤ 5.0	278	5.2
5	> 5.0	20	0.4
	Total:	5340	100

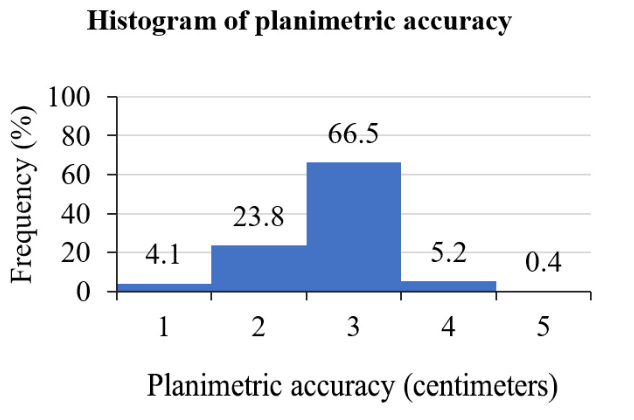

b) GPT_{Dry} with GMF_{Dry}

	Planimetric Accuracy (centimeters)	Frequency	
		Units	(%)
1	≤ 0.5	221	4.1
2	> 0.5 and ≤ 1.0	1201	22.5
3	> 1.0 and ≤ 3.0	3582	67.1
4	> 3.0 and ≤ 5.0	315	5.9
5	> 5.0	21	0.4
	Total:	5340	100

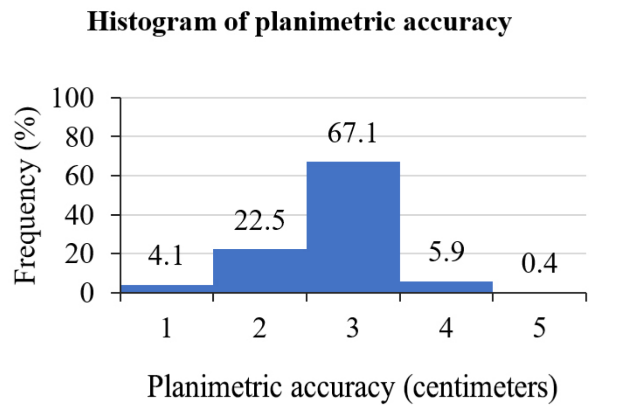

c) $ECMWF_{Dry}$ with $VMF1_{Dry}$

	Planimetric Accuracy (centimeters)	Frequency	
		Units	(%)
1	≤ 0.5	226	4.2
2	> 0.5 and ≤ 1.0	1266	23.7
3	> 1.0 and ≤ 3.0	3540	66.3
4	> 3.0 and ≤ 5.0	286	5.4
5	> 5.0	22	0.4
	Total:	5340	100

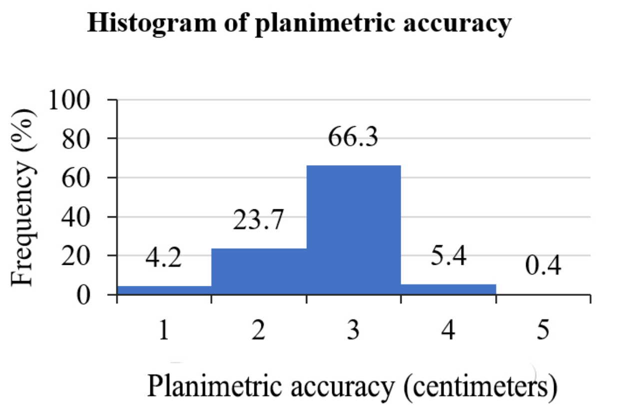

Figure 3. Histograms of planimetric accuracy samples (A) for strategy 4: $Saastamoinen_{Dry}$ with NMF_{Dry}; (B) for strategy 5: GPT_{Dry} with GMF_{Dry}; (C) for strategy 6: $ECMWF_{Dry}$ with $VMF1_{Dry}$.
Figura 3. Histogramas das amostras de acurácia planimétrica (A) para estratégia 4: $Saastamoinen_{Dry}$ com NMF_{Dry}; (B) para estratégia 5: GPT_{Dry} com GMF_{Dry}; (C) para estratégia 6: $ECMWF_{Dry}$ com $VMF1_{Dry}$.

A histogram was created with the six samples of planimetric accuracy in order to emphasize the relative comparison between the various strategies for mitigating the tropospheric delay.

It can be seen in Figure 4 that most of the planimetric accuracy sample was above 1 cm and below 3 cm in all tropospheric models evaluated. It could be seen that, in relation to the accuracy of the planimetric result, the tropospheric refraction models presented similar results.

Frequency histograms of altimetric accuracy are presented below for each tropospheric delay model (Figures 5 and 6). Figure 4A represents frequency histogram of altimetric accuracy in which a priori model for hydrostatic component of tropospheric delay was not used during processing. It can be noted that 100% of sample showed an accuracy value greater than 5 cm, reaching 49 centimeters. Figure 5B presents another frequencies histogram of altimetric accuracy for strategy 1. In this histogram, the class intervals are different from the others, in order to help interpretation of altimetric accuracy values in PPP when a priori model for correcting hydrostatic component is not used. According to this new histogram (Figure 5B), 85.4% of altimetric accuracy sample were greater than 15 cm, and approximately half of the samples reached values greater than 20 cm, which show the significant effects that tropospheric delay can cause on the altimetric component, unlike what happens with planimetric component. The frequency histogram of altimetric accuracy for strategy 2 is shown in Figure 5C. The a priori model used to correct hydrostatic component was the Saastamoinen, and the NMFwet mapping function was applied to the estimated wet component. Figure 4C shows that 56.8% of samples had altimetric accuracy values below 3 cm. On the other hand, 15.5% of results were greater than 5 cm (5 to 27 cm).

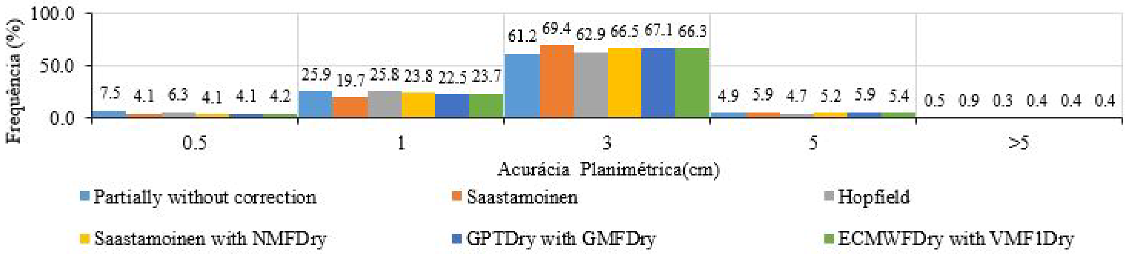

Figure 4. Total Histogram of planimetric accuracy samples.
Figura 4. Histograma total das amostras de acurácia planimétrica.

Figure 6A represents frequency histogram of altimetric accuracy of strategy in which a priori Hopfield model was used to analyze hydrostatic component, and Hopfield mapping function for estimated wet component. It can be seen in Figure6A that only 21.1% of samples presented values below 3 cm when a priori Hopfield model is used in PPP processing. In addition, 52.5% of results were greater than 5 cm, reaching up to 22 cm. Figure6B represents frequency histogram of altimetric accuracy for the processing using a priori Niell model ($Saastamoinen_{Dry}$ in conjunction with the NMF_{Dry} mapping function), and NMFWet mapping function for wet component. As result, 76% of altimetric accuracy samples showed values below 3 cm. Values greater than 5 cm (5 to 16 cm) were obtained by 9% of samples. Frequency histogram in Figure 6C represents altimetric accuracy of strategy 5. The a priori model used at processing was the GPTDry, the GMFDry mapping function was applied for hydrostatic component, and the GMFWet for wet component. Figure 6C shows that 76.6% of values were smaller than 3 cm, and 9% of samples obtained altimetric accuracy greater than 5 cm (0.05 to 0.16 m).

Frequency histogram of altimetric accuracy presented at Figure6D represents the processing in which a priori $ECMWF_{Dry}$ model was used in conjunction with $VMF1_{Dry}$ mapping function. For the wet component, the VMF1Wet mapping function was used. When analyzing Figure 6D, we can see that 76.8% of histogram values were below 3 cm. In addition, only 8.7% of sample showed values greater than 5 cm (5 to 16 cm). Thus, we can infer that using a priori ECMWF model associated with $VMF1_{Dry}$ mapping function presented the best performance among strategies used for analyzing altimetric accuracy, since its application returned the lowest percentages of values above 5 cm and the highest percentage below 3 cm. However, results presented by the last three strategies were similar. Xu & Xu (2016) highlight that VMF1 mapping function is the one that provides best results globally. In addition, these authors claim that GMF mapping function can provide results consistent with those provided by VMF1 function, which was verified in this study (see Figures 6C and 6D). The performance of NMF mapping function is worth mentioning, since it had also provided similar results (Figure 6B). This function is not suitable for polar regions (latitudes greater than 75 degrees - north and south) (Xu & Xu, 2016), which makes it important to emphasize that no GNSS station located in these regions was used in this study.

a) Partially without correction

	Altimetric accuracy (centimeters)	Frequency Units	Frequency (%)
1	≤ 0.5	0	0
2	> 0.5 and ≤ 1.0	0	0
3	> 1.0 and ≤ 3.0	0	0
4	> 3.0 and ≤ 5.0	0	0
5	> 5.0	5340	100
	Total:	5340	100

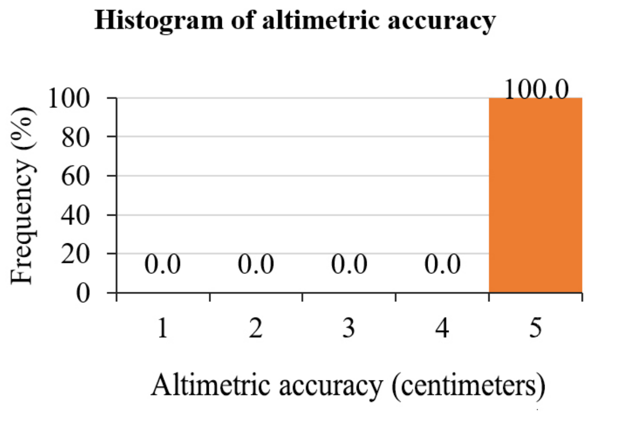

b) Partially without correction

	Altimetric accuracy (centimeters)	Frequency (%)	Frequency (%)
1	≤ 0.5	780	14.6
2	> 0.5 and ≤ 1.0	2011	37.7
3	> 1.0 and ≤ 3.0	1391	26
4	> 3.0 and ≤ 5.0	837	15.7
5	> 5.0	321	6
	Total:	5340	100

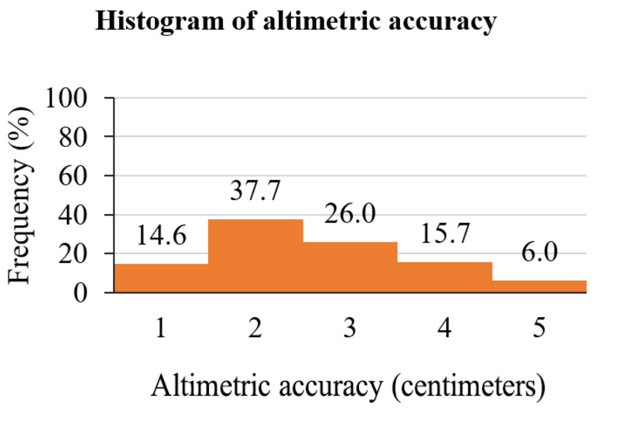

c) Saastamoinen

	Altimetric accuracy (centimeters)	Frequency Units	Frequency (%)
1	≤ 0.5	465	8.7
2	> 0.5 and ≤ 1.0	516	9.7
3	> 1.0 and ≤ 3.0	2050	38.4
4	> 3.0 and ≤ 5.0	1479	27.7
5	> 5.0	830	15.5
	Total:	5340	100

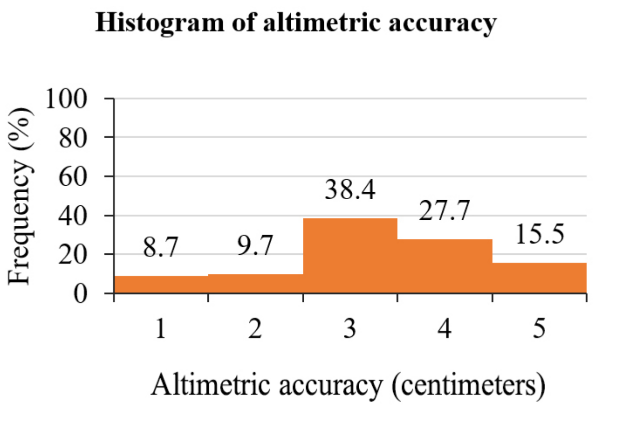

Figure 5. Histograms of altimetric accuracy samples. (A) for strategy 1: Partially without correction; (B) for strategy 1: Partially without correction with different intervals; (C) strategy 2: Saastamoinen.

Figura 5. Histogramas das amostras de acurácia altimétrica (A) para estratégia 1: Parcialmente sem correção; (B) para estratégia 1: Parcialmente sem correção para diferentes intervalos; (C) para estratégia 2: Saastamoinen.

a) Hopfield

	Altimetric accuracy (centimeters)	Frequency Units	Frequency (%)
1	≤ 0.5	78	1.5
2	> 0.5 and ≤ 1.0	106	2
3	> 1.0 and ≤ 3.0	942	17.6
4	> 3.0 and ≤ 5.0	1411	26.4
5	> 5.0	2803	52.5
	Total:	5340	100

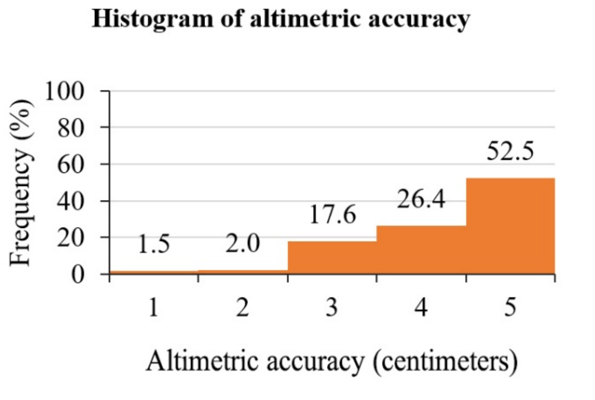

b) Saastamoinen$_{Dry}$ with NMF$_{Dry}$

	Altimetric accuracy (centimeters)	Frequency Units	Frequency (%)
1	≤ 0.5	768	14.4
2	> 0.5 and ≤ 1.0	809	15.1
3	> 1.0 and ≤ 3.0	2481	46.5
4	> 3.0 and ≤ 5.0	801	15
5	> 5.0	481	9
	Total:	5340	100

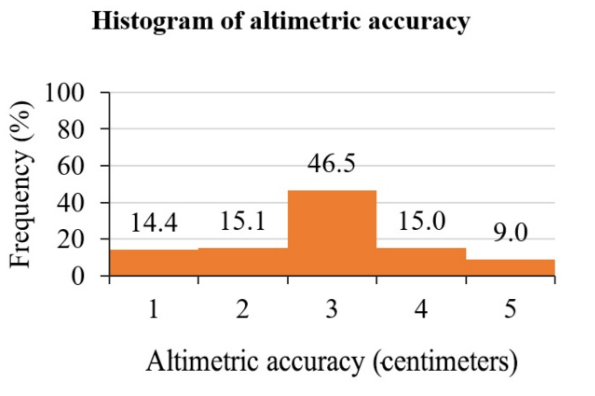

c) GPT$_{Dry}$ with GMF$_{Dry}$

	Altimetric accuracy (centimeters)	Frequency Units	Frequency (%)
1	≤ 0.5	785	14.7
2	> 0.5 and ≤ 1.0	821	15.4
3	> 1.0 and ≤ 3.0	2482	46.5
4	> 3.0 and ≤ 5.0	773	14.5
5	> 5.0	479	9
	Total:	5340	100

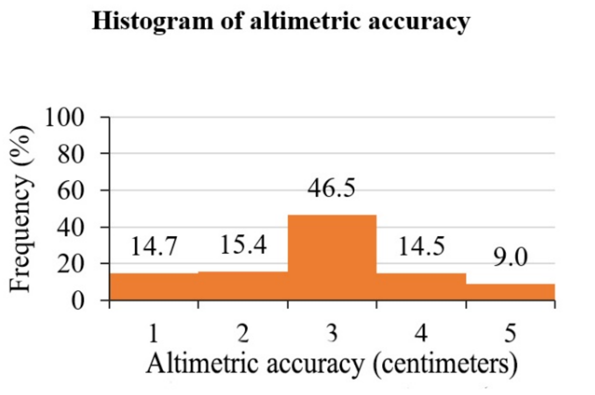

d) ECMWF$_{Dry}$ with VMF1$_{Dry}$

	Altimetric accuracy (centimeters)	Frequency Units	Frequency (%)
1	≤ 0.5	786	14.7
2	> 0.5 and ≤ 1.0	791	14.8
3	> 1.0 and ≤ 3.0	2525	47.3
4	> 3.0 and ≤ 5.0	773	14.5
5	> 5.0	465	8.7
	Total:	5340	100

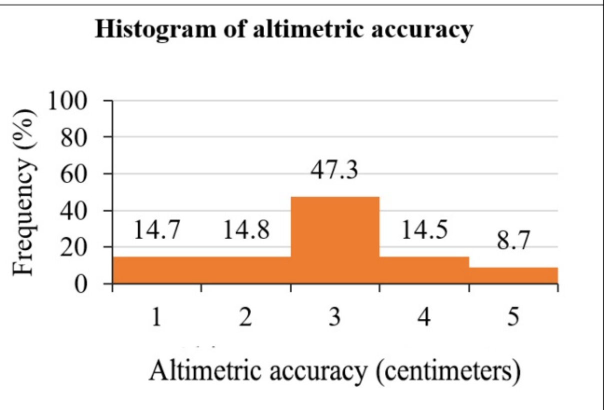

Figure 6. Histograms of altimetric accuracy samples (A) for strategy 3: Hopfield; (B) for strategy 4: Saastamoinen$_{Dry}$ with NMF$_{Dry}$; (C) for strategy 5: GPT$_{Dry}$ with GMF$_{Dry}$;(D) for strategy 6: ECMWF$_{Dry}$ with VMF1$_{Dry}$.

Figura 6. Histogramas das amostras de acurácia altimétrica (A) para estratégia 3: Hopfield; (B) para estratégia 4: Saastamoinen$_{Dry}$ com NMF$_{Dry}$; (C) para estratégia 5: GPT$_{Dry}$ com GMF$_{Dry}$; (D) para estatégia 6: ECMWF$_{Dry}$ com VMF1$_{Dry}$.

A histogram was created with the six samples of altimetric accuracy in order to emphasize the relative comparison between the various strategies for mitigating the tropospheric delay.

Analyzing Figure 7, the Hopfield model did not present a different performance than the other processing strategies for the altimetric accuracy samples. It is also noted that in the model partially without tropospheric correction, 100% of the sample was greater than 5 cm. The GPT/GMF, Niell, ECMWF/VMF1 models showed similar results.

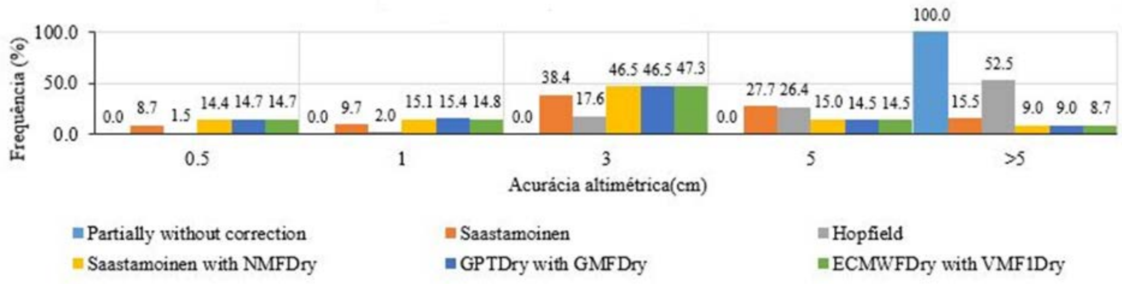

Figure 7. Total Histogram of altimetric accuracy samples.
Figura 7. Histograma total das amostras de acurácia altimétrica.

3.1 Influence of Seasonal Variation and Climate Zone on Altimetric Component

Tropospheric delay is strongly correlated with estimated height, thus predominantly affecting accuracy of altimetric component (Dach *et al.*, 2015). In this sense, this study chose to evaluate only the behavior of altimetric accuracy, considering both season and climatic zone of the place under study. The Root Mean Square (RMS) of altimetric accuracy for the 15 days of processing in summer, autumn, winter and spring periods was calculated for each a priori model used in this study. In addition, these RMS values were divided according to Brazilian climate domains: 1-Tropical Central Brazil, 2-Temperate, 3-Equatorial, 4-Tropical Equatorial and 5-Tropical Eastern Notheast (Figure 8). Figure 8A represents RMS of altimetric accuracy given by application of strategy 1, in meters, according to analyzed period and climatic region. As in this processing strategy a priori model was not used to correct hydrostatic component of tropospheric delay, RMS values varied between 15 to 27 cm.

RMS values for GNSS stations located in Equatorial climate zone were higher than those of the other climatic domains. This climatic zone is strongly influenced by Amazon region, which has high annual humidity values. In fact, Anderson & Strahler (2008) defines in their study the wet equatorial climate, which encompasses a good part of Equatorial climate zone shown in Figure 1. Rainfall is abundant and regular so that the region has the rainiest climatic regime in Brazil (Nimer, 1989). On the other hand, Nimer (1989) also highlights that in equatorial zone there is a less rainy corridor, from the Roraima state to east of the Pará state, passing through middle area of Amazon state. This corridor can contribute to a greater variation in precipitation in this region, as well as to a variation in humidity. In other words, the rainfall regime is not homogeneous in this region, contrary to what happens with temperature. This scenario increases the difficulty of estimating wet component of tropospheric delay using a mapping function, as already mentioned. Results obtained show that marked variability of humidity in equatorial zone compromises wet component estimation process, therefore also compromising PPP accuracy. However, it is believed that with the deforestation of the Amazon forest, in the future there will be a decrease in the region humidity, which will cause, consequently, higher temperatures and drier climates (Rohll & Veja, 2018). If this happens, PPP performance is expected to be better and similar to the results obtained in the other climatic zones.

GNSS stations located in the Temperate climate domain, on the other hand, had the lowest RMS values in all seasons of the year under study. Nimer (1989) highlights that in this climatic zone there is a more homogeneous process of distribution of precipitations, and consequently of humidity, which contributes to better performance of PPP in this region. In addition, for all climatic regions, the highest RMS values were obtained in the summer and spring (Figure 8A).

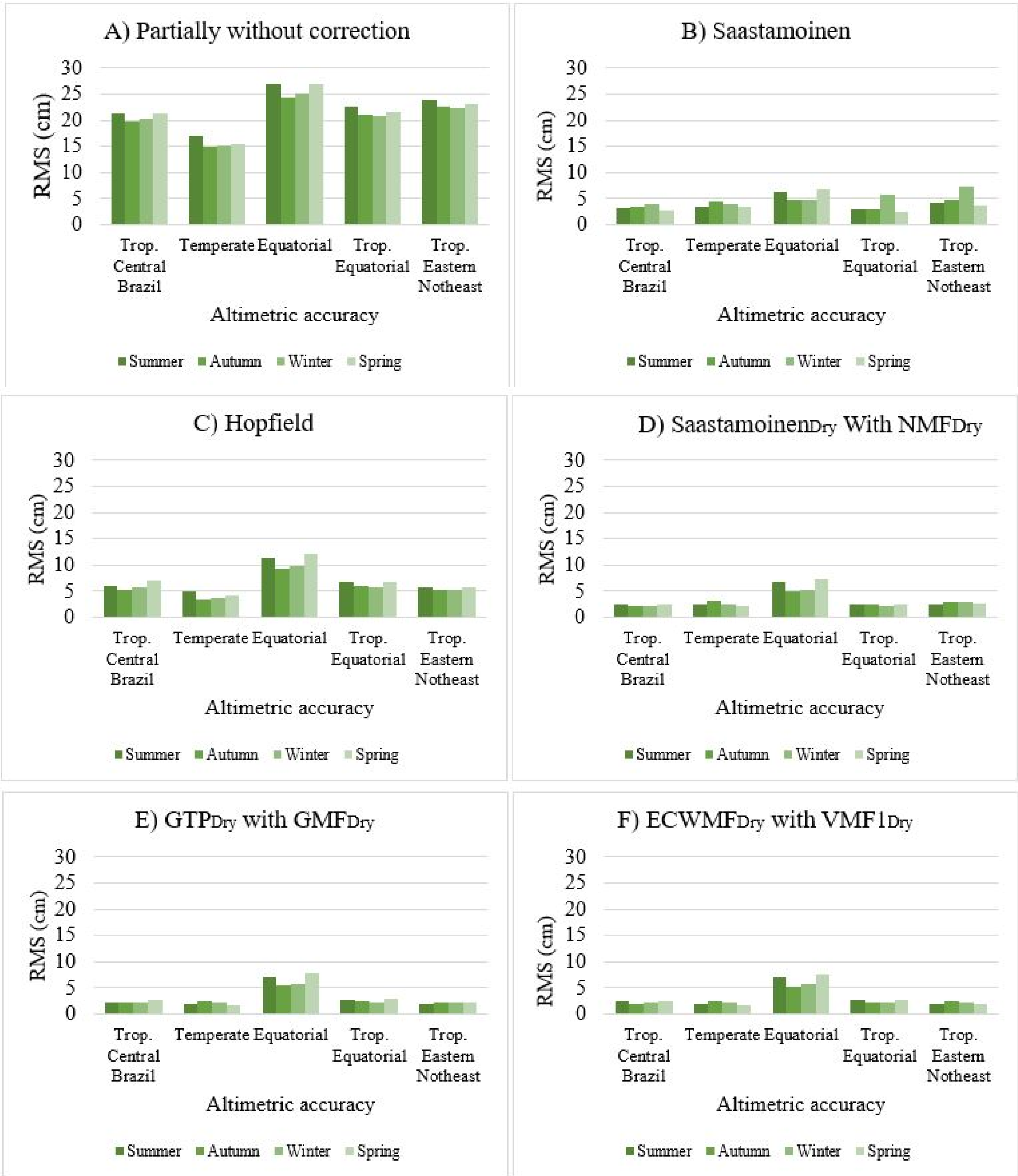

Figure 8. RMS (in meters) of altimetric accuracy by climatic zones and processing strategy (A) Partially without correction; (B) Saastamoinen; (C) Hopfield; (D) Saastamoinen$_{Dry}$ with NMF$_{Dry}$; (E) GPT$_{Dry}$ with GMF$_{Dry}$; (F) ECMWF$_{Dry}$ with VMF1$_{Dry}$.

Figura 8. RMS (em metros) da acurácia altimétrica por zonas climáticas e por estratégia de processamento (A) Parcialmente sem correção; (B) Saastamoinen; (C) Hopfield; (D) Saastamoinen$_{Dry}$ com NMF$_{Dry}$; (E) GPT$_{Dry}$ com GMF$_{Dry}$; (F) ECMWF$_{Dry}$ com VMF1$_{Dry}$.

RMS for strategy 2 are shown in Figure 8B. There is a significant improvement when using a priori model. Among the 20 possibilities, considering all climatic zones and seasons, in only 4 cases the RMS exceeded 5 cm. Equatorial climatic zone presented highest RMS values for altimetric accuracy in summer and spring. However, the highest RMS was obtained in Tropical Eastern Northeast zone in winter, reaching up to 7.5 cm.

Figure 8C represents RMS of altimetric accuracy for processing strategy 3. In general, strategy 3 provided higher RMS values when compared to the second one. As with the first processing strategy, all RMS were larger in Equatorial climate zone, for all seasons, reaching approximately 12 cm in the spring. Likewise, lowest RMS values were obtained in Temperate zone. In addition, for all climatic regions, RMS values were lower in autumn and winter.

Figures 8D, 8E and 8F show results obtained by applying strategies 4, 5 and 6, respectively. As strategies application generated similar results, the figures will be analyzed together. With the exception of the results for Equatorial zone, these strategies showed the best results, considering all seasons. Their RMS values hovered around just 2.5 cm. In comparison, strategy 2 showed better results in Equatorial zone, although the difference is not accentuated. Again, for the last three strategies the largest RMS occurred in Equatorial zone, reaching approximately 7.5 cm in the winter. It is important to highlight the influence of hydrological loading in GNSS stations located near the Amazon River (Equatorial zone), mainly the NAUS station, as verified by Nascimento *et al.* (2017). Thus, this station was not used for data processing. It is also noteworthy that it was not possible to identify a pattern in relation to the seasons, except for the Equatorial zone: in all processing strategies, the worst results to that zone were obtained in summer and spring, periods of the most intense rain regime.

5 Conclusions

Experiments of this study were carried out for 89 RBMC stations distributed along the five climatic zones of Brazil, in a 15 days interval for each season of 2016. Processing parameters of evaluated strategies were standardized, so that comparisons could be made. Six processing strategies for modeling tropospheric delay in PPP were analyzed. The models for tropospheric refraction applied to verify planimetric accuracy of the coordinates had a very similar performance, compared to the performance of the models applied to analyze altimetric component, even in the processing in which a priori tropospheric model was not used. This confirmation proves that troposphere effects are not significant at planimetry level. On the other hand, strategy 2, which used a priori Saastamoinen model for ZHD and Niell wet mapping function for ZWD, obtained the lowest percentage of frequencies of planimetric accuracy below 3 cm (93.28%) and the highest percentage of the sample with planimetric accuracy greater than 5 cm (0.86%).

In relation to altimetric component, the application of the strategy in which a priori tropospheric model was not used, in which only the ZWD estimate was performed, resulted in accuracy values around 7 to 49 cm, much higher than any other processing. In this case, it appears that tropospheric delay considerably affects accuracy of estimated height of GNSS stations, if this parameter is not corrected in the data processing, when considering the PPP methodology. Hopfield model, despite having a result similar to that of other strategies when analyzing planimetric accuracy, did not obtain the same success in relation to altimetric accuracy, since its application resulted in 52.49% of sample with altimetric accuracy greater than 5 cm. This inferior result when analyzing altimetric component was also found in study by Dodo *et al.* (2010), who evaluated tropospheric models in a regional GNSS network in Africa, using BSW. In this study, when Hopfield model was used in processing, RMS of altimetric component was equal to 5 cm in all analyzed GNSS stations. Processing based on Saastamoinen model for ZHD and Niell wet mapping function for ZWD (strategy 2) also showed a lower performance compared to the other strategies, with only 56.76% of altimetric accuracy frequencies below 3 cm. It should be noted that Hopfield and Saastamoinen models are empirical and were obtained based on meteorological observations collected predominantly in the northern hemisphere.

Considering the characteristics of this study, it was found that the best GNSS Positioning Technique to verify altimetric component is the use of VMF1 (Dry) mapping function, by Böhm *et al.* (2006b), in conjunction with ZTD corrections based on the ECMWF Numerical Weather Forecast model, with 94.2% of the sample accuracy less than 3 cm. It is also noted that RMS of altimetric accuracy varied according to climatic zone and the epoch of GNSS data gathering. As a country of continental dimensions, Brazil has different topographic and climatic characteristics. Therefore, final coordinates of GNSS stations over the Brazilian territory experience different influences from tropospheric delay.

For future work, it is recommended to use multiple years of GNSS data processing, in addition to time series analysis of positional accuracy. Since the Brazilian climatology is very variable, in addition to the seasons, in relation to the years, there may be an increase or decrease in humidity in the same periods of different years, which would directly impact the ZWD and consequently the accuracy of the PPP.

Acknowledgments. The authors would like to thank the Coordenação de Aperfeiçoamento de Pessoal de Nível Superior – Brasil (CAPES) – Financing Code 001, for the scholarship granted to the first author. The authors also thank IBGE for the availability of RBMC data.

Referências

Abreu, P.A.G, Alves, D.B.M. & Gouveia, T.A.F. 2014. Aplicação e avaliação do modelo de Previsão Numérica do Tempo Eta15km no posicionamento absoluto. *Rev Bras Cartogr*, 66(3): 555-567.

Alves, D.B.M., Sapucci, L.F., Marques, H.A., de Souza, E.M., Gouveia, T.A.F. & Magário, J.A. 2016. Using a regional numerical weather prediction model for GNSS positioning over Brazil. *GPS solutions*, 20(4): 677-685.

Anderson, B.T. & Strahler, A. 2008. *Visualing weather and climate*. New Yok, John Wiley & Sons, 528p.

Bar-sever, Y.E, Kroger, P.M. & Borjesson, J.A. 1998. Estimating horizontal gradients of tropospheric path delay with a single GPS receiver. *J Geophys Res*, 103: 5019-5035.

Böhm, J.; H. Schuh. 2004. Vienna mapping functions in VLBI analyses. *Geophysical Research Letters*, 31: L01603.

Böhm, J., Niell, A., Tregoning, P. & Schuh, H. 2006a. Global Mapping Function (GMF): A new empirical mapping function based on numerical weather model data. *Geophys Res Lett*, 33: L07304.

Böhm, J., Werl, B. & Schuh, H. 2006b. Troposphere mapping functions for GPS and very long baseline interferometry from European Centre for Medium-Range Weather Forecasts operational analysis data. *J Geophys Res*, 111: B02406.

Böhm, J.; Heinkelmann, R.; Schuh, H. 2007. Short note: A global model of pressure and temperature for geodetic applications. *J Geod*, 81(10): 679-683.

Bos M. & Scherneck H.G. 2013. Computation of Green's Functions for Ocean Tide Loading. *In:* Xu G. (Eds) *Sciences of Geodesy - II*. Springer, Berlin, Heidelberg.

Bruyninx, C., Altamimi, Z., Caporali, A., Kenyeres, A., Lidberg, M., Stangl, G. & Torres, G.A. 2013. *Guidelines for EUREF Densifications*. IAG sub-commission for the European Reference Frame.

Chen, G. & Herring, T.A. 1997. Effects of atmospheric azimuthal asymmetry on the analysis of space geodetic data. *J Geophys Res*, 102: 20489-20502.

Chuerubim, M.L., Segantine, P.C.L. & Silva, I. 2016. O impacto dos modelos troposféricos no posicionamento GNSS de alta precisão em diferentes épocas e estações do ano. *Rev de Engenharia e Tecnologia*, 8(2): 44-54.

Collins, P. & Langley, R.B. 1999. Tropospheric Delay. *GPS World*, 1: 52-58.

Costa, S.M.A.; Junior, E.S.F.; Fazan J.A.; Monico, J.F.G. & Camargo, P.O. 2002. Preliminary Results of SIRGAS 2000 Campaign —IBGE Analysis Center. *In:*

Drewes H., Dodson A.H., Fortes L.P.S., Sánchez L., Sandoval P. (Eds) *Vertical Reference Systems. International Association of Geodesy Symposia*, Springer, vol 124. Berlin, Heidelberg, p 306-311.

Dach, R., Simon, L., Walser, P. & Fridez, P. 2015. *User manual of the Bernese GNSS. Software 5.2*, Switzerland: AIUB, 852p.

Davis, J.L., Herring, T.A., Shapiro, I.I., Rogers, A.E.E. & Elgered, G. 1985. Geodesy by radio interferometry: effects of atmospheric modeling errors on estimates of baseline length. *Radio Sci*., 20(6): 1593-1607.

Dodo, J.D. & Idowu, T.O. 2010. Regional Assessment of the GPS Tropospheric Delay Models on the African GNSS Network. *J Emerging Trends Eng Appl Sci*, 1: 113-121.

Foelsche, U. & Kirchengast, G. 2002. A simple‘‘geometric’’mapping function for the hydrostatic delay at radio frequencies and assessment of its performance. *Geophys Res Lett*, 29: 1111-1114.

Gouveia, T.A.F., Alves, D.B.M. & Sapucci, L.F. 2017. Avaliação da acurácia e tempo de convergência do PPP com o uso de previsão numérica de tempo na modelagem do atraso troposférico. *Rev Bras Cartogr*, 69: 433-445.

Gouveia, T.A.F., Sapucci, L.F., Monico, J.F.G., & Alves, D.B.M. 2014. Avaliação robusta da modelagem neutrosférica sobre o território brasileiro baseada em modelos de Previsão Numérica de tempo da América do Sul. *Bol de Ciênc Geod*, 20: 481-503.

Herring, T.A. 1992. Modelling atmospheric delays in the analysis of space geodetic data, In: symposium on refraction of transatmospheric signals in geodesy. *Netherlands Geod. Commis*, 36: 157-164.

IERS Conventions. 2010. Gérard Petit and Brian Luzum (eds.). *IERS Technical Note 36*. Frankfurt am Main: Verlag des Bundesamts für Kartographie und Geodäsie, 2010. 179 p.

Ifadis, I. 1986. The atmospheric delay of radio waves: Modeling the elevation dependence on a global scale. *In:* TECHNICAL REPORT N°. 38L, School of Electrical and Computer Engineering, Chalmers University of Technology, Goteborg, Sweden.

IGN. Institut National de L'Information Géographique et Forestière. 2017. Available at: < https://itrf.ign.fr/trans_para.php >. Date of Access: Feb. 16, 2017.

Karabatic, A. & Weber, R. 2009. Precise Point Positioning (PPP) - an alternative processing technique to estimate the tropospheric wet delay of GNSS signals. *Geophysical Research Abstracts*, 11: EGU2009-4492.

Landskron, D. & Böhm, J. 2017. VMF3/GPT3: Refined discrete and empirical troposphere mapping functions. *J Geod*, 92: 349-360.

Marini, J.W. 1972.Correction of satellite tracking data for an arbitrary tropospheric profile. *Radio Sci*, 7: 223-231.

Monico, J.F.G. 2008. *Posicionamento pelo GNSS: Descrição, fundamentos e aplicações*. 2.ed. São Paulo: Editora UNESP, 476 p.

Nascimento, L.A., Dal Poz, W.R., Santos, A.P. & Freitas, K.X.S. 2017. Geração automatizada de séries temporais de dados posicionais utilizando o IBGE-PPP. *Bol de Ciênc Geod*, 23: 150-165.

Niell, A. 1996. Global mapping functions for the atmosphere delay at radio wavelengths. J Geophys Res, 101: 3227-3246. https://doi.org/10.1029/95JB03048.

Nimer, E.1979. Um modelo metodológico de classificação de climas [A methodological model of climate classification]. *Rev Bras de Geogr*, 41(4): 59-89.

Nimer, E. 1989. *Climatologia do Brasil. Rio de Janeiro, IBGE, Departamento de Recursos Naturais e Estudos Ambientais*. Rio de Janeiro, 422p.

Oliveira, A.F., Alves, D.B.M. & Ferreira, L.D.D. 2014. Avaliação de Diferentes Modelos Troposféricos de Previsão Numérica de Tempo no Posicionamento em Redes. *Rev Bras Cartogr*, 66(3): 691-704.

Pan, L. & Guo, F. 2018. Real-time tropospheric delay retrieval with GPS, GLONASS, Galileo and BDS data. *Sci. Rep.*, 8: 17067.

Ray, R.D. & Ponte, R.M. 2003.Barometric tides from ECMWF operational analyses. *Ann Geophys*, 21: 1897–1910.

Rohli, R.V. & Veja, A.J. 2018. *Climatology*. Burlington, Massachusetts, Jones & Bartlett Learning, 418p.

Saha, K., Raju, C.S. & Parameswaran, K. 2010. A new hydrostatic mapping function for tropospheric delay estimation. *J Atmos Sol Terr Phys*, 72: 125-134.

Saastamoinen, J. 1972. Atmospheric correction for the troposphere and stratosphere in radio ranging of satellites. the use of artificial satellites for geodesy. *Geophys Monogr*, 15: 247-251.

Sanz-Subirana, J., Juan Zornoza, J.M. & Hernández-Pajares, M. 2013. *GNSS Data Processing, Volume I: Fundamentals and Algorithms*. Noordwijk, ESA Communications, ESTEC, 223p.

Spilker Jr, J.J. 1996.Tropospheric Effects on GPS. In: PARKINSON BW & SPILKER Jr JJ. Global Positioning System: theory and applications. Washington, AIAA. *Progress in Astronautics and Aeronautics*: 517-546.

Sapucci, L.F. & Monico, J.F.G. Avaliação dos modelos de Hopfield e de Saastamoinen para a modelagem do atraso zenital troposférico em território brasileiro utilizando GPS. *In: Séries em Ciências Geodésicas 30 anos de Pós-Graduação em Ciências Geodésicas no Brasil*. Curitiba, Vol. 1, p.47-61, 2001.

Seeber, G. 2003. *Satellite Geodesy: foundations, methods and applications*. 2.ed., Berlin, New York: Walter de Gruyter, 589p.

Teunissen, P.J.G. & Kleusberg, A. 1998. *GPS for Geodesy*. Berlin, Springer-Verlag. 640 p.

Torge, W. & Müller, J. 2012. *Geodesy*. 4th Edition, Walter de Gruyter, Berlin. 444p.

Tunali, E. & Özlüdemir, M.T. 2019. GNSS PPP with different troposphere models during severe weather conditions. *GPS Solutions*, 23: 1-11.

VMF1. *Vienna Mapping Function*. 2017. Available at: https://vmf.geo.tuwien.ac.at/trop_products/GRID/2.5x2/VMF1/VMF1_FC/. Date of Access: Nov. 27, 2017.

Waldhelm, R., Gomes, I.P., Ventura, R.N., Trindade, R.T., & Bretas, R. 2006. *Projeto Infra-estrutura Geoespacial Nacional-PIGN*.

Wang, M. & Li, B. 2016. Evaluation of empirical tropospheric models using satellite-tracking tropospheric wet delays with water vapor radiometer at Tongji, China. *Sensors*, 16: 1-15.

Weston, N.D. & Soler, T. *Rigorous Geodetic Positioning in the Americas*. 13p, 2012. Available at: <https://www.ngs.noaa.gov/CORS/Articles/Weston-SolerFIG-2012-Montevideo.pdf>. Date of Access: March 22, 2017.

Xiong, C., Lu, L. & Zhao, L. 2019. Analysis on the Impacts of Slant Tropospheric Delays on Precise Point Positioning. *Appl Sci*, 9.22: 4884.

Xu, G. & Xu, Y. 2016. *GPS: Theory, Algorithms and Applications*. Berlin, Springer, 489p.

Zhao, Q., Yao, Y., Yao, W., & Li, Z. 2018. Real-time precise point positioning-based zenith tropospheric delay for precipitation forecasting. *Sci Rep*, 8: 7939.

Manuscrito 118014	Recebido em ago de 2021	Aceito em jul de 2022	Editor: Felipe G. Nievinski